Supplementary Materials and Methods

Plant materials

The *abi1-1* (Leung et al., 1994), *pyr1;pyl1;pyl2;pyl4* (Park et al., 2009), *aba2-1* (Gonzalez-Guzman et al., 2002), *tir1-1;afb2-3;afb4-8;afb5-5* (NASC, (Prigge et al., 2016)), *scr3* (Fukaki et al., 1998), *shr2* (Helariutta et al., 2000). *p35S::PYR1^{MANDI}* (Park et al., 2015), *pSCR::abi1-1/pUAS::abi1-1* (Duan et al., 2013), *35S::Iaa6m1m2* (Li et al., 2011), *pS18::ER-GFP* (Lee et al., 2006), *pVND7::YFP-NLS* (Kubo et al., 2005), *pAHP6::GFP-ER* (Bishopp et al., 2011), *pMIR165a::GFP/pMIR166b::GFP* (Carlsbecker et al., 2010), *pPHB::PHB-GFP/pPHB::GFP-ER* (Miyashima et al., 2011), *DR5::Venus-NLS* (Heisler et al., 2005), *DII-Venus* (Brunoud et al., 2012), and *zll/pZLL::YFP:ZLL* (Tucker et al., 2008) are in *Col-0*. The *phb-13;phv-11;cna-2* (Prigge et al., 2005) is in the *Col (er2)* and *phb-1d* (McConnell et al., 2001) is in the *Ler*. For tissue-specific expression various enhancer trap lines were crossed to plants harboring *pUAS::abi1-1*. For control experiments the *C24* background was crossed to *pUAS::abi1-1*. Analyses were done on F1 generation of crosses as previously described (Duan et al., 2013). To evaluate the effect of mandipropamid on *miR165-GFP* expression, homozygous *p35S::PYR1^{MANDI}* and *pMIR165a::GFP* transgenes were crossed and analyzed in F1 progeny.

Growth conditions

Seeds were surface-sterilized by vapor-phase sterilization in a closed container with 6 ml concentrated HCl (32%) added to 100 ml bleach (11%) for 1.5-2 hours and ventilated for 15 min in sterile environment. Seeds were sown on standard plates containing 0.5X Murashige & Skoog (0.5X MS) salt mixture (Sigma M5519) titrated to pH 5.7 with MES and KOH, 1% sucrose, and 0.8% agar and vernalized for 2 days at 4 °C. Plates were transferred to a growth chamber and grown vertically under long-day conditions (16 h light/8 h dark cycles) at 21 °C. The light intensity was 100 $\mu E \cdot m^{-2} \cdot s^{-1}$.

Cell length measurements

Confocal images were acquired with Zeiss Plan-Apochromat 20X/0.8 M27 objective as tile-scan in the middle section of roots. Cell lengths measurements were carried out with semi-automated Cell-o-Tape, ImageJ (Fiji) macro (Band et al., 2012). All measurements were done on the cortex cell layer with numbering starting from the first initial adjacent to the QC. The position of the ETZ for each root was first estimated automatically by the built-in TSZ feature in Cell-o-Tape and then confirmed manually by the requirement that at least three adjacent cells had a minimum of 20% increase in cell length. Size of the elongation zone (e.g., exit to maturation) was calculated on cortex cells starting from ETZ until the position at which the first root hair emerged. In *Col-0* it is usually eight or nine cells.

Confocal microscopy

Images were captured on Zeiss LSM 780-NLO laser-scanning confocal microscope with Plan-Apochromat 20X/0.8 and C-Apochromat 40X/1.20 W Korr FCS objectives (Zeiss). For time-lapse experiments LD Plan-Neofluar 40X/0.6 was used. Emission was detected with GaAsP spectral detector. Imaging settings were as follows: PI, excitation with 561 nm diode laser and emission between 590-650 nm; GFP, excitation with argon laser at 488 nm and emission between 505-545 nm; Venus, excitation with argon laser at 514 nm and emission between 520-560 nm; calcofluor white, excitation with 405 nm diode laser and emission between 420-470 nm; basic fuchsin, excitation with 561 nm diode and emission between 580-640 nm. For simultaneous detection of PI and Venus, spectral separation lambda mode was used with 514 nm argon excitation and emission set between 520-600 nm with 8.9-nm step intervals. In lateral roots high levels of autofluorescence were detected even after clearing, thus for separation of autofluoresence from GFP signal in LRI spectral separation lambda mode was used with 488 nm argon excitation and emission set between 500-550 nm with 8.9-nm step intervals. Image analyses were performed with Fiji and Zeiss ZEN10.

Gene expression by quantitative RT-PCR

For analysis of gene expression *Col-0*, *abi1-1*, and *pyr1;pyl1;pyl2;pyl4* 5-DAG seedlings were treated with 10 µM ABA or 0.1% ethanol liquid solution in 0.5X MS for 1 h. *p35S::PYR1*^{MANDI} 5-DAG seedlings were treated with 10 µM mandipropamid or 0.1% methanol for 3 h. For 24-h treatments *Col-0* 5-DAG seedlings were transferred to plates supplemented with 10 µM ABA or 0.1% ethanol. Tissue was collected from 60-70 roots for each genotype and treatment. The first 0.5 cm of root (close to root tip) was dissected under a dissecting microscope and used for RNA extraction. Total RNA was extracted with miRNeasy Micro Kit (Qiagen, 217084) and treated with DNase (Qiagen, 79254) to eliminate possible DNA contamination. Total RNA (0.5 µg per sample) was used for reverse transcription with High Capacity cDNA Reverse Transcription Kit (Applied Biosystems, 4368814). For quantitative RT-PCR, Fast SYBR Green Master Mix (Applied Biosystems, 4385612) was used in 15-µl reactions. Cycles were run on Applied Biosystems StepOnePlus PCR system. Three-stage PCR reactions were done with three technical replicates and annealing at 60 °C. *PP2A* (*At1G13320*) expression is stable under ABA treatments and was used as a reference for normalization of the data. At least three biological replicates were done for each genotype and treatment, and representative experiments are presented in figures.

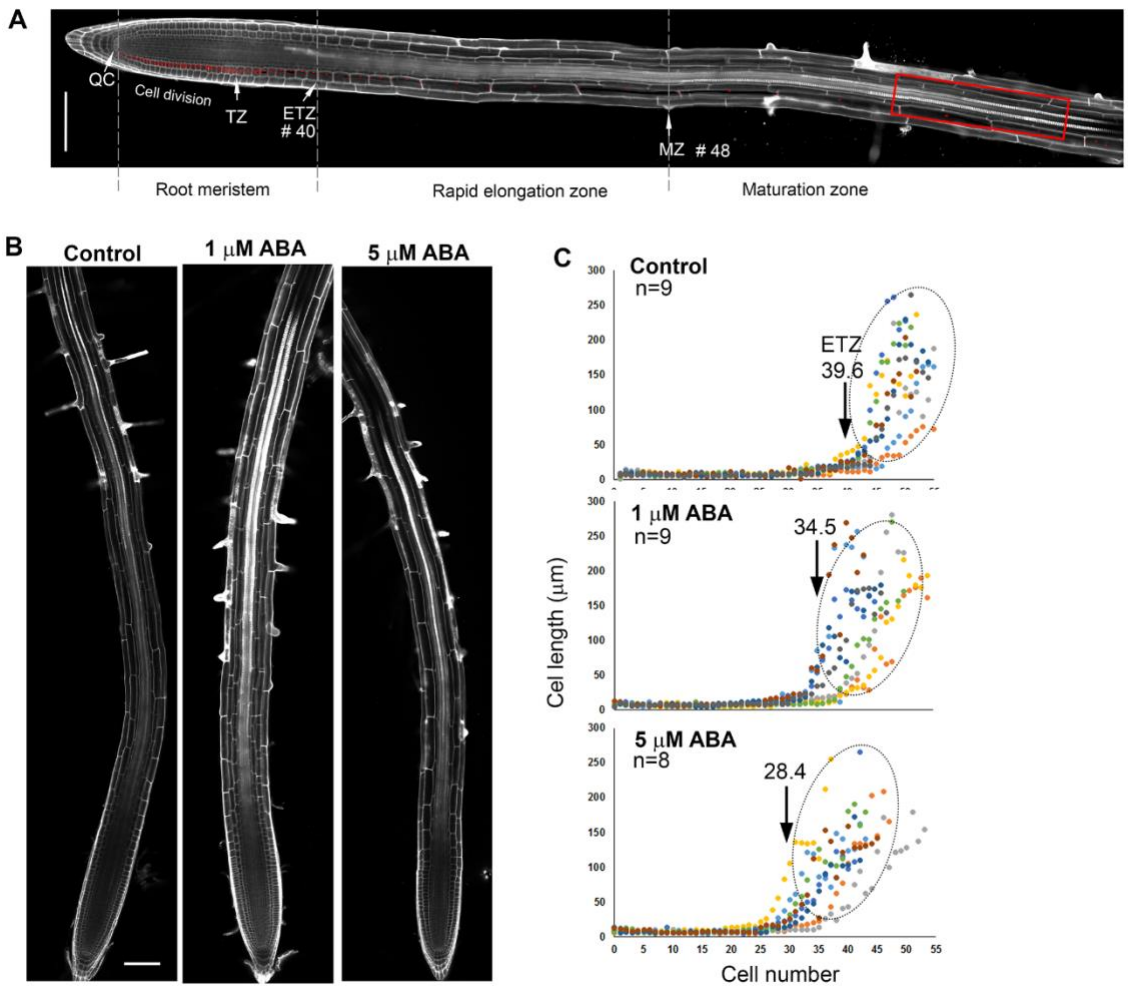

Fig. S1. **Response of the primary root to ABA.** *(A)* A tile scan image of a *Col-0* WT primary root stained with PI. Cortex cell numbers marked in red. Meristematic zone includes dividing and transiently amplifying (transition zone) cells, around 40 cells in WT. The end of the transition zone (ETZ) defines the beginning of rapid cell elongation zone. The position of root hair emergence relative to ETZ defines the size the elongation zone (8-9 cells in WT) and characterizes the rate of root maturation/differentiation. QC, quiescence center; TZ, start of the transition zone; ETZ, end of transition zone; MZ, initiation of the maturation zone determined by the appearance of root hair cells. Red rectangle marks the region where morphology of vascular tissues was analyzed: 3-4 cells distal to the first root hair cell or 11-13 cells from the ETZ. (*B*) Primary roots following 24-h treatment with the indicated concentrations of ABA. EtOH treatment served as a control. Cell walls were stained with PI. (*C*) Cell length analysis, starting from QC, following 24-h treatment with ABA. Independent roots (n) are presented in different colors. Numbers and arrows mark the average positions of the ETZ. Note the response of roots to ABA with regard to meristem size (position of ETZ) and cell length distributions at the elongation/maturation zone (ellipses). Scale bars in panels *A* and *B*, 100 μm.

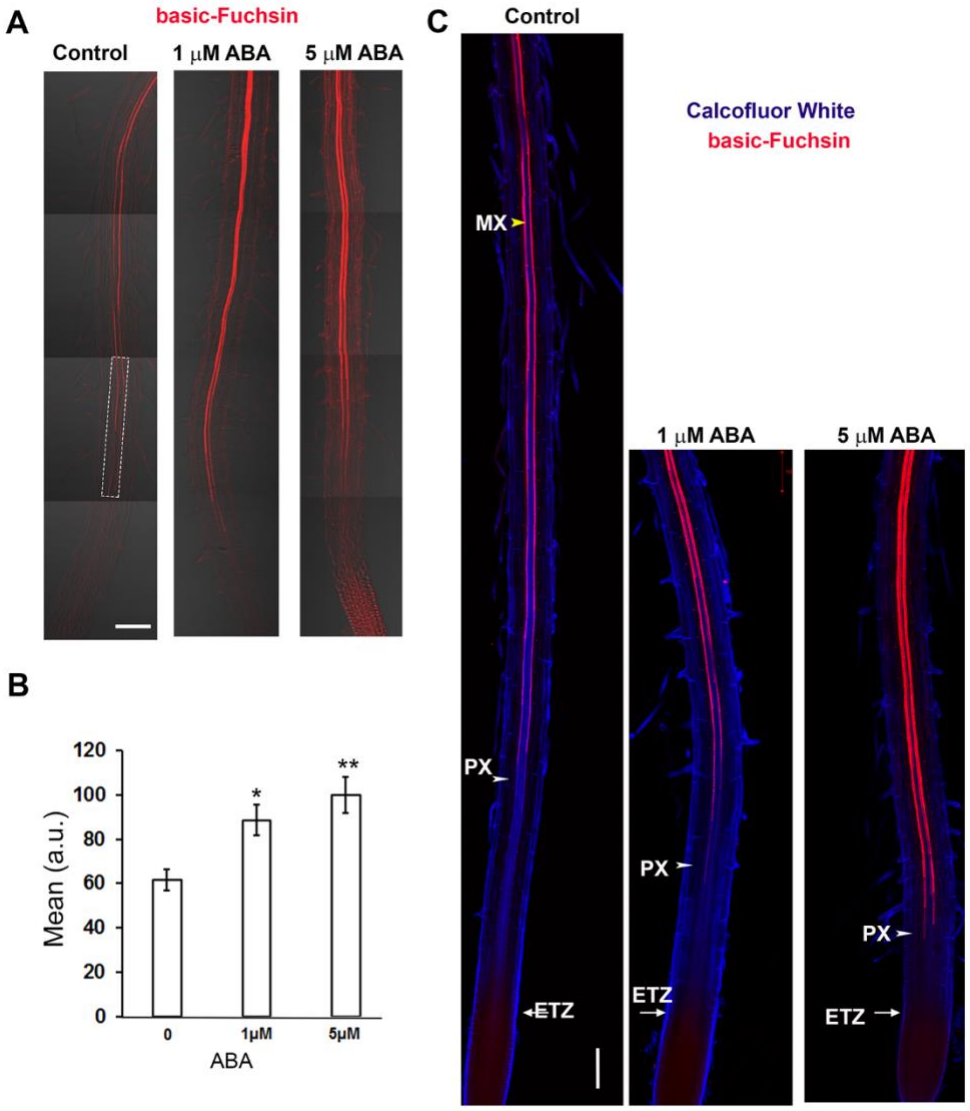

Fig. S2. **Effect of ABA on xylem lignification.** (*A*) Tile images of *Col-0* roots stained with basic-fuchsin (red) following 24-h incubation in control or ABA-containing media. The white rectangle defines the region where measurements were performed. Scale bar, 100 µm. (*B*) Bar graph presenting the mean fluorescent intensity of fuchsin in vascular tissue of the maturation zone (n = 6 per treatment). Error bars are SE. Statistically significant differences (*p≤ 0.05; ** p≤ 0.005) relative to controls were computed based on the Student's t-tests, two-tail distribution, unequal variance. (*C*) Double staining of primary cell walls of cleared *Col-0* roots with calcofluor white (blue) and lignified SCW with basic-fuchsin (red). Note the difference between position of PX and MX differentiation at control conditions and earlier lignification of PX after ABA treatments. Scale bar, 100 µm.

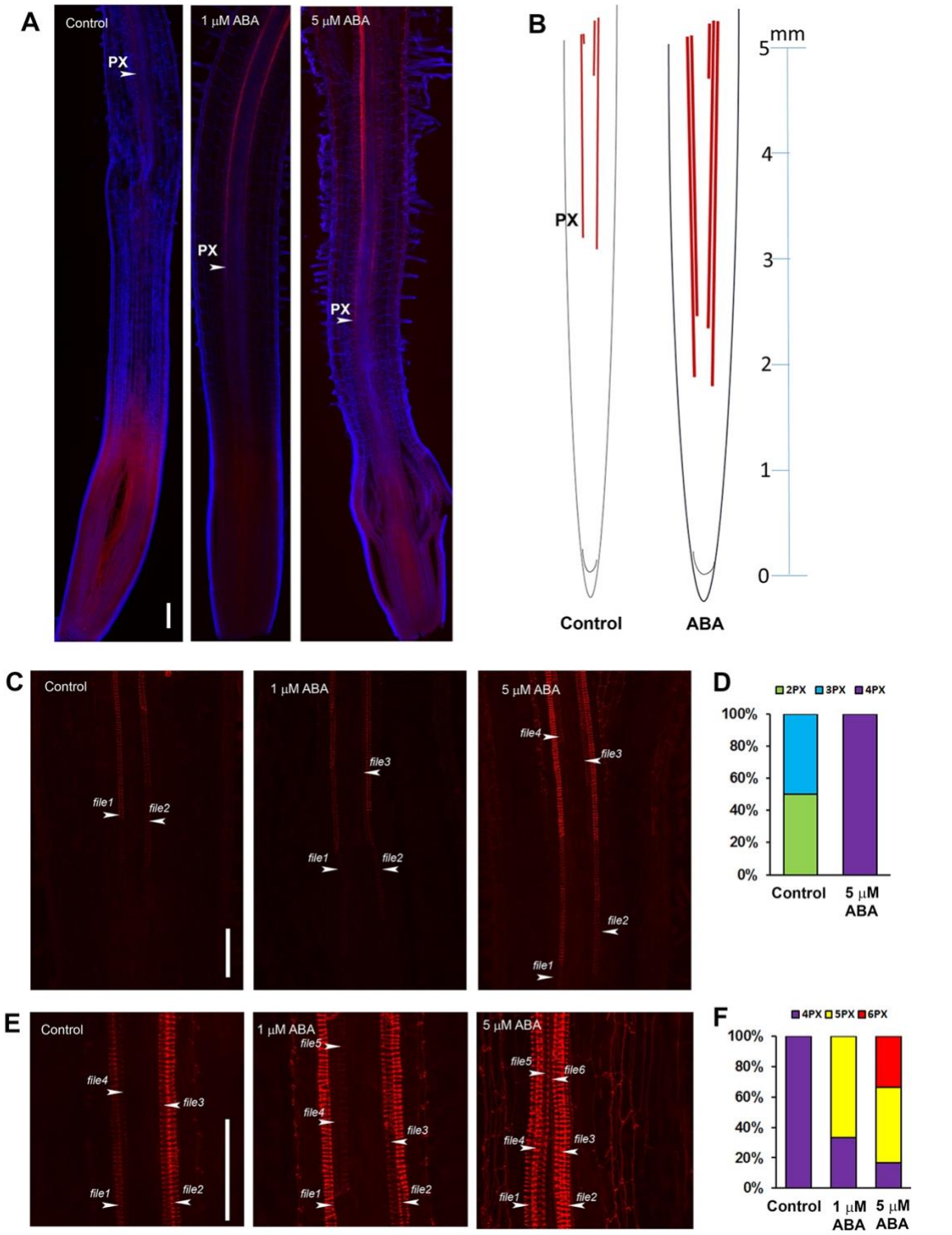

Fig. S3. **Effects of ABA on PX differentiation in tomato.** (*A*) Tomato (*Solanum lycopersicum* M82) roots treated with ethanol (control) or with ABA at indicated concentrations for 48 hours, cleared and stained with calcofluor white (blue) and basic-fuchsin (red). The position of PX is defined. *(B)* A scheme displaying the effect of ABA treatments on PX differentiation. Note that tomato roots have 4 PX cell files two of which differentiate 2-3

mm from the tip and the second pair about 5 mm from the tip. ABA induces earlier differentiation of all 4 PX files and formation of additional PX files about 5 mm form the tip. *(C)* Close-up view of first lignified PX cell files in differentiation region of *M82* tomato root. Lignified PX cell files are indicated with white arrowheads. Images are Z-stack maximal projections. *(D)* Frequencies of PX cell file numbers in differentiation region of the root in control or ABA treated conditions (n=4 in control, n=5 in 5 µM ABA). *(E)* Close-up view of PX in the mature root region at distance of around 5 mm form root tip. Lignified PX cell files are indicated with white arrowheads. Images are Z-stack maximal projections. *(F)* Frequencies of PX cell file numbers in mature region of root in control or ABA treated conditions (n=4 in control, n=6 in 1 µm and 5 µM ABA). Scale bars in panels *A*, *C* and *E*, 100 µm.

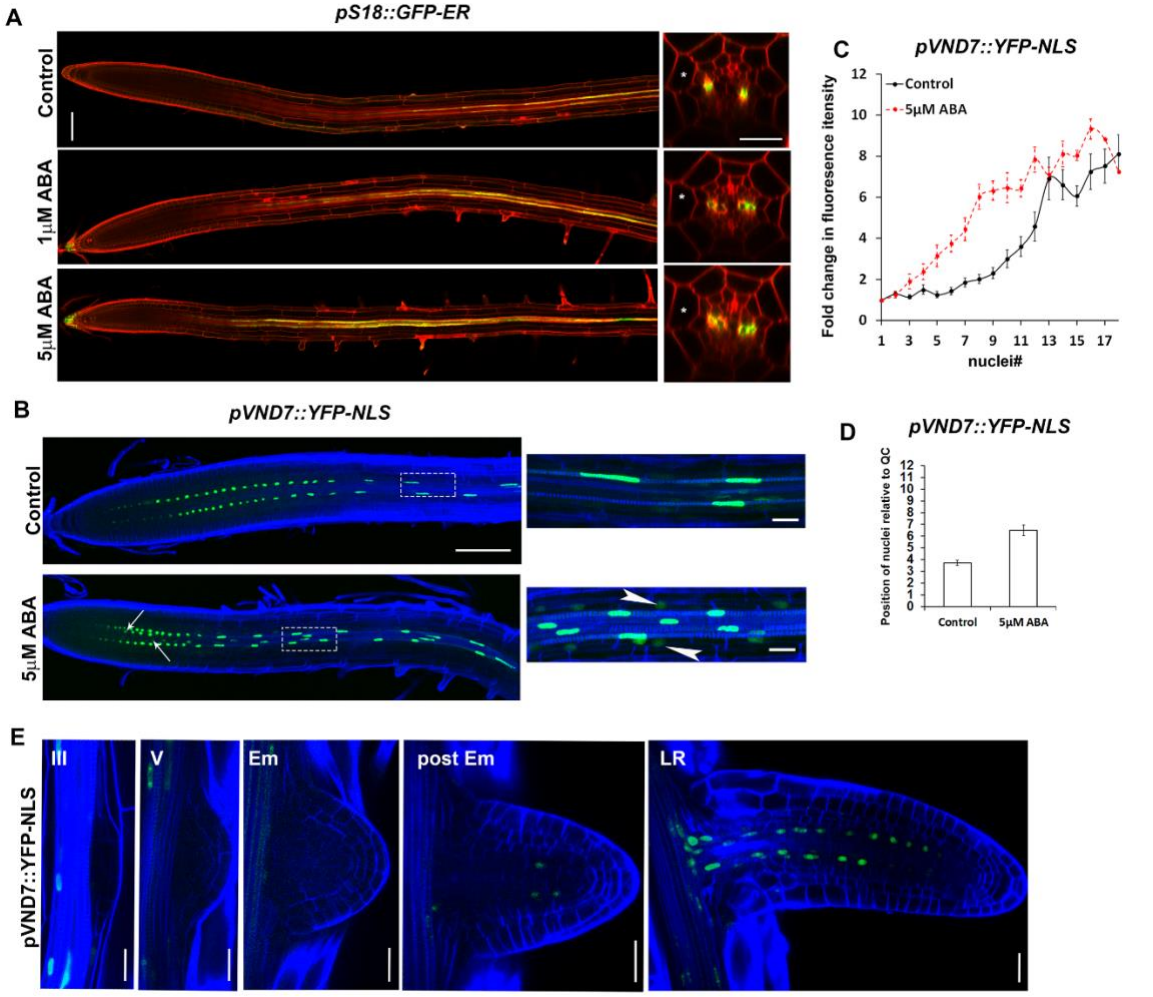

Fig. S4. **Effect of ABA on expression of PX differentiation markers.** *(A)* Expression of the maturing PX marker *pS18::ER-GFP* (green) following 24-h treatment with ABA or with EtOH as a control. Cell walls were stained with PI (red). Asterisks indicate endodermis. *(B)* Expression of *pVND7::YFP-NLS* (green) in cleared roots stained with calcofluor white (blue) after treatment with 5 µM ABA or with EtOH as a control. Arrows indicate additional cell files of xylem cells expressing YFP-NLS. Rectangles mark regions in the elongation zone enlarged at the right. Arrowheads indicate spreading of VND7 expression to pericycle after ABA treatment. *(C)* Mean fold change in YFP-NLS nuclear signal intensity relative to the expression levels in the first nucleus. Values on x-axis are nuclei numbers starting from the first nuclei with expression. Note that ABA treatments induce fast increase in *pVND7::YFP-NLS* expression levels compared to control treatments were VND7 expression increased gradually in the first nine nuclei. (n= 18 cell files per treatment). *(D)* Position of the first *pVND7::YFP-NLS* positive nuclei in PX provascular cells relative to QC after ABA and EtOH (Control) treatments (n=18 cell files per treatment). (*E*) pVND7::YFP-NLS expression in lateral roots. Stages of development are indicated. Em – emergence. Scale bars 100 µm in panel *A* left images and 20 µm for Z-stacks at the right, 100 µm in panel *B* left images and 10 µm in magnifications on the right and 20 µm in E. Error bars, SE.

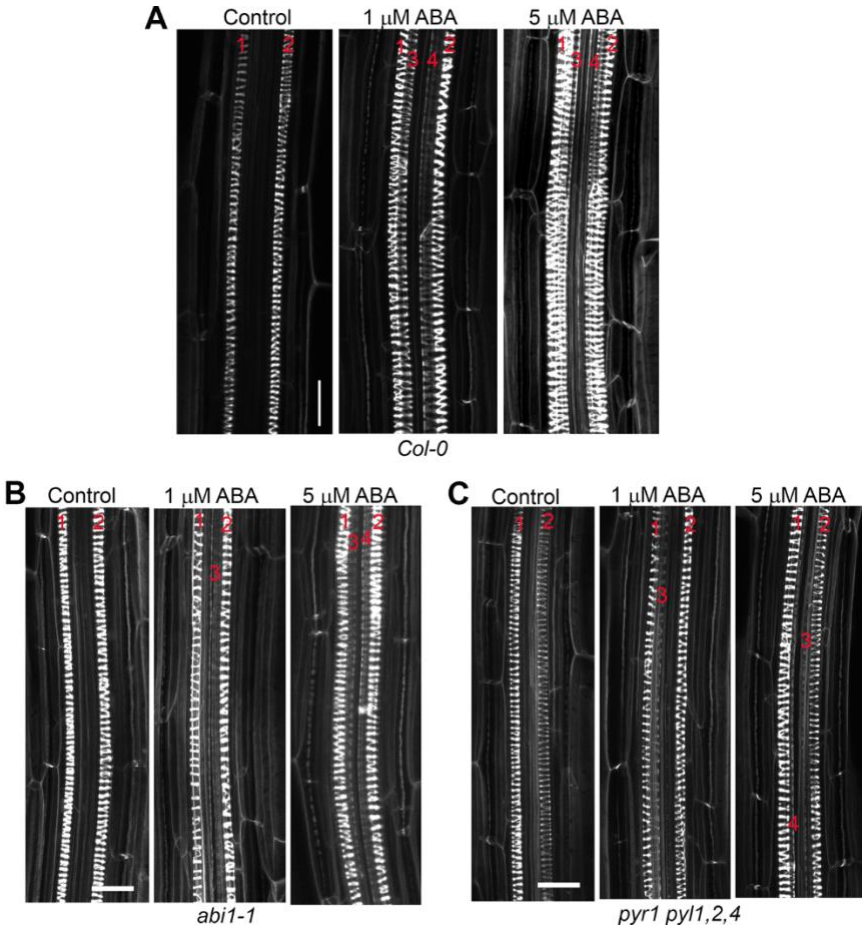

Fig. S5. **Formation of extra PX cell files is suppressed in ABA signaling mutants.** Z-stack maximal projections of roots in (*A*) WT, (*B*) *abi1-1*, and (*C*) *pyr1;pyl1;pyl2;pyl4* mutant seedlings treated with ABA. Note that additional files of PX (red digits) in *abi1-1* and *pyr1;pyl1;pyl2;pyl4* mutants treated with ABA have less defined and weakly stained spiral SCW patterns. Cell walls were stained with PI (white). Scale bars, 20 μm.

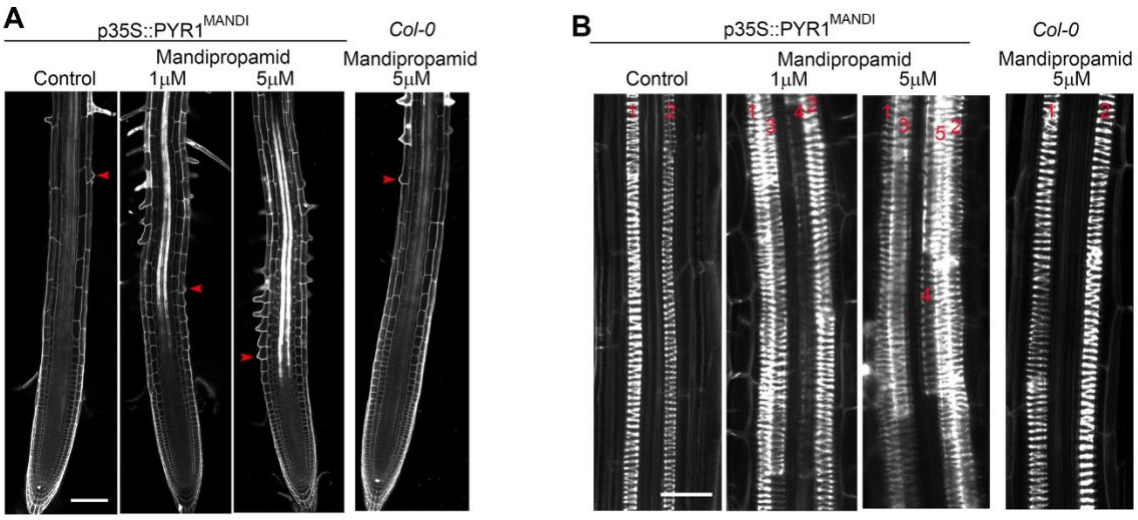

Fig. S6. **Mandipropamid treatment of *p35S:PYR1^{MANDI}* seedlings induces formation of extra PX.** *(A)* Roots of *p35S:PYR1^{MANDI}* and *Col-0* (WT) plants treated with mandipropamid for 24 h. Red arrowheads mark the position of the first emerging root hairs. Scale bar, 100 µm. *(B)* Z-stack maximal projections of roots of *p35S:PYR1^{MANDI}* and *Col-0* seedlings treated with 1 or 5 µM mandipropamid. Mandipropamid induced differentiation of four or five PX files (red digits), respectively, in *p35S:PYR1^{MANDI}* but not in WT control roots. Scale bar, 20 µm. Cell walls were stained with PI (white).

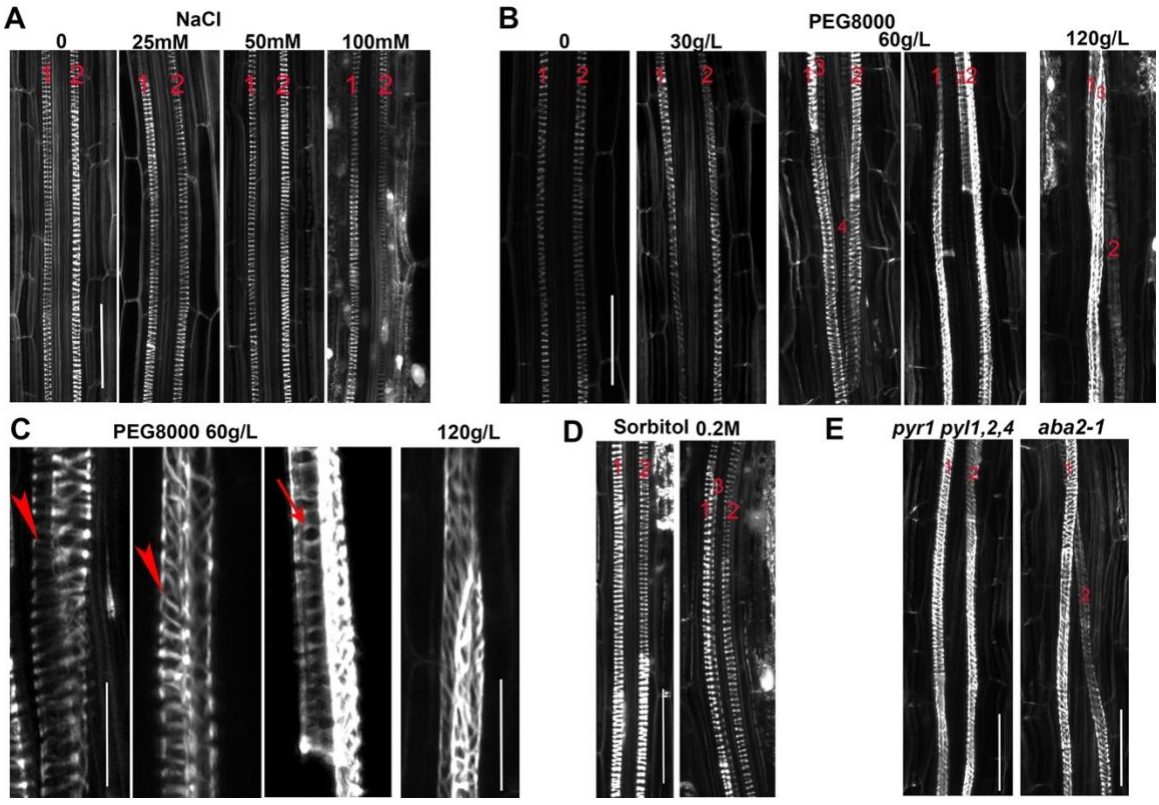

Fig. S7. **Effect of salt and osmotic stress on xylem development in WT and ABA mutants.** *(A)* Xylem architecture after 24-h treatments with the indicated concentrations of NaCl. Only two PX files are observed at all concentrations. *(B)* Xylem structure 24 h after treatments with the indicated concentrations of PEG 8000. Additional PX files were detected following treatments with 60 g/L and 120 g/L. *(C)* Close-up view of *Col-0* xylem cells treated with PEG 8000. The secondary cell wall patterns in xylem are disorganized with some similar to PX (arrowheads); others form atypical MX (arrow). Note the strong effect on secondary cell wall patterning in the 120 g/L PEG 8000-treated roots. *(D)* Xylem structure after 24-h treatments with 0.2 M sorbitol. Additional PX files are observed. *(E)* Xylem architecture of *aba2-1* and *pyr1;pyl1;pyl2;pyl4* mutants following treatments with 60g/L PEG-8000. Images show roots that do not form additional PX cell files. All images are Z-stack maximal projections of vascular tissue. Cell walls were stained with PI. Numbers indicate xylem cell files. Scale bars in panels *A*, *B*, *D*, and *E*, 20 µm; in panel *C*, 10 µm.

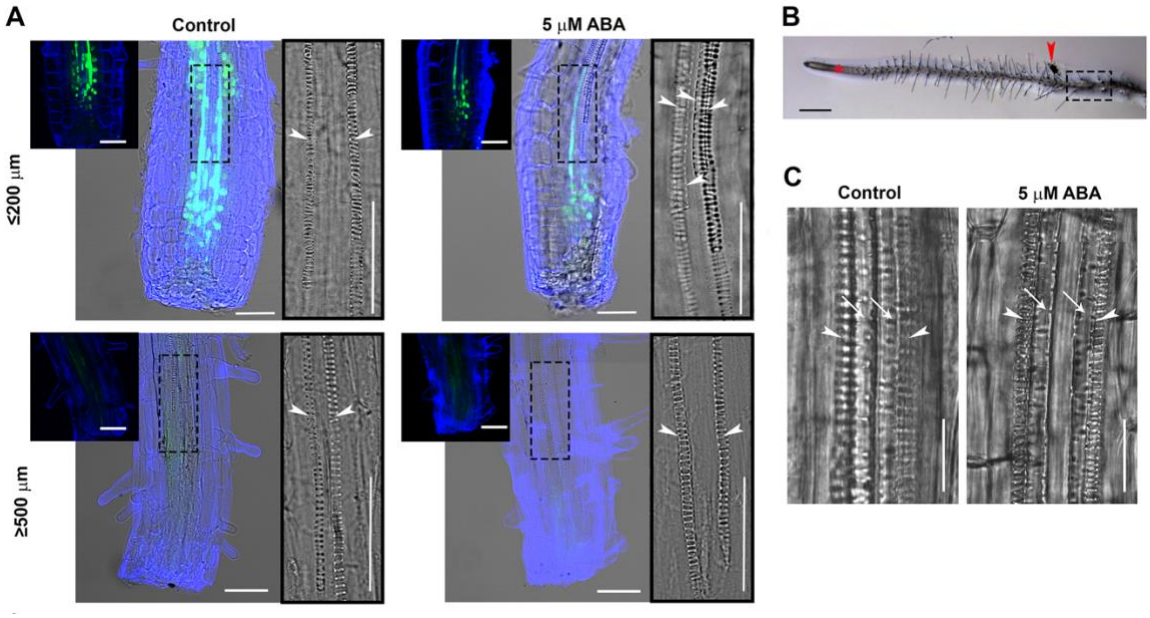

Fig. S8. **Meristem function is required for ABA-induced formation of PX.** Roots were excised at distances ≤200 μm or ≥500 μm from the tip. Alternatively, the roots were labeled at the initiation of the elongation zone. Xylem development was examined after 24 h. Cell walls were stained with calcofluor white (blue). *(A)* DIC images of cleared calcofluor white-stained (blue) *DR5::Venus-NLS* (green) roots following excisions at distances ≤ 200 μm or ≥ 500 μm from the tip and subsequent 24-h treatment with solvent control or 5 μM ABA. Insets, fluorescent images displaying the regenerating auxin maximum (green) in excised tips. Rectangles, regions of enlarged DIC xylem imaging (right). Arrowheads indicate PX. *(B)* Roots were labeled at the initiation of elongation zone (red asterisk indicates the original position of coal relative to root meristem). Red arrowhead marks the position of the label after 24 h. Dashed rectangle highlights the region of enlarged DIC image displayed in panel *C*. *(C)* DIC images displaying xylem differentiation in the region defined by dashed rectangle in panel *B*. Arrowheads indicate PX; arrows, MX. Scale bars in panel *A*, 50 μm; in panel *B*, 500 μm; and in panel *C*, 20 μm.

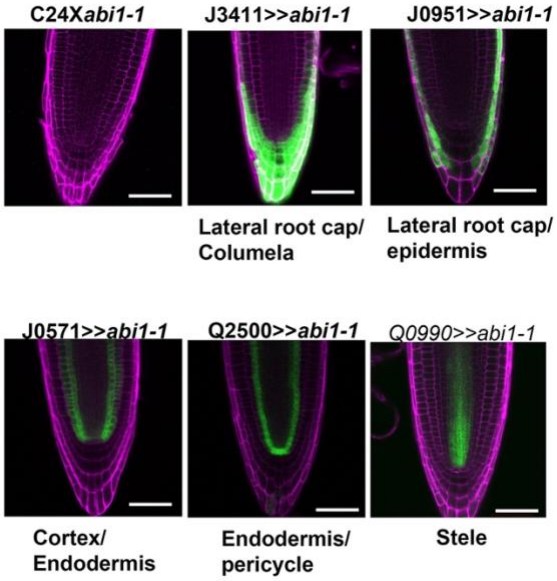

Fig. S9. **Tissue-specific expression of enhancer trap lines crossed to *pUAS::abi1-1*.** (*A*) Confocal images of primary roots of *pUAS::abi1-1* crossed to enhancer trap lines and C24 background, for control, in F1 progeny. Cell walls were stained with PI (magenta). (B) Expression of stele/endodermis and cortex/endodermis-specific *pUAS::abi1-1* lines Q2500 and J0571, respectively in cleared lateral root initials at stage V and emergence (Em). Cell walls were stained with calcofluor white (blue). Activity domain of GAL4 enhancer trap lines was visualized by GFP (green). Scale bars, 50 µm in A and 20 µm B.

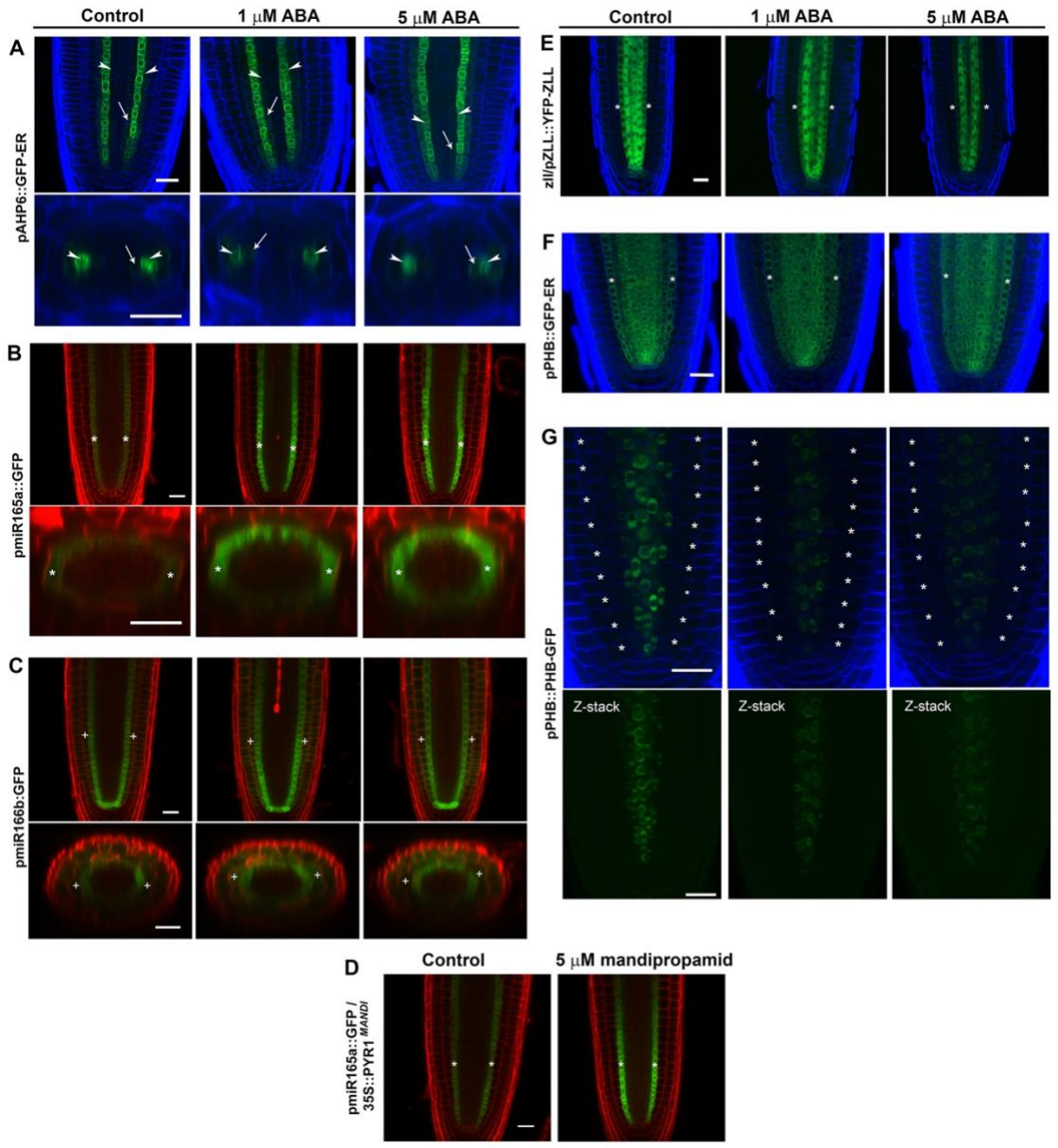

Fig. S10. **ABA alters radial patterning regulators in the meristem.** *(A) pAHP6::GFP-ER* expression (green) in root meristem of cleared roots following 24 h treatments with indicated concentrations of ABA and ethanol for control. Lower panels are Z-cross sections. Note that expression was detected in PX (arrowhead) and at low levels in pericycle and MX (arrow). *(B)* Expression of *pmiR165a::GFP-ER* (green) in root meristem following 24 h treatments with indicated concentrations of ABA and ethanol for control. Asterisks mark the endodermis. Lower panels are Z-cross sections. *(C)* Expression of *pmiR166b::GFP-ER* (green) in root meristem following 24 h treatments with indicated concentrations of ABA and ethanol for control. + indicates cortex. Lower panels are Z-cross sections. *(D)* Expression of *pmiR165a::GFP-ER* (green) in *p35S:PYR1*^{MANDI} background treated with control (ethanol) or 5 μM mandipropamid for 24 h. Asterisks mark

the endodermis. *(E) zll/pZLL::YFP-ZLL* expression (green) in root meristem of cleared roots following 24 h treatments with indicated concentrations of ABA and ethanol for control. Asterisks mark the endodermis. *(F) pPHB::GFP-ER* expression (green) in cleared root meristem following 24 h treatments with indicated concentrations of ABA and ethanol for control. Asterisks mark the endodermis. *(G)* Single scans through the middle of root meristem displaying expression of *pPHB::PHB-GFP* (green) in cleared root tips following 24 h treatments with indicated concentrations of ABA and ethanol for control. Asterisks mark the endodermis. Lower panels Z-stack maximal projections. Note that both PHB-GFP expression levels and the size of expression domain are reduced under ABA treatments. In panels *A*, *E*, *F*, and *G* cell walls in cleared roots were stained with calcofluor white (blue). In panels *B-D*, roots were stained without clearing with PI (red). Fluorescence of GFP/YFP-based reporters is shown in green. Scale bars, 20 μm. In box plots, x indicates the mean, lines indicate the median. Error bars, SE. Statistically significant differences relative to controls (*$p \leq 0.05$; ** $p \leq 0.005$; *** $p \leq 0.0005$) were computed based on the Student's t-tests, two-tail distribution, unequal variance.

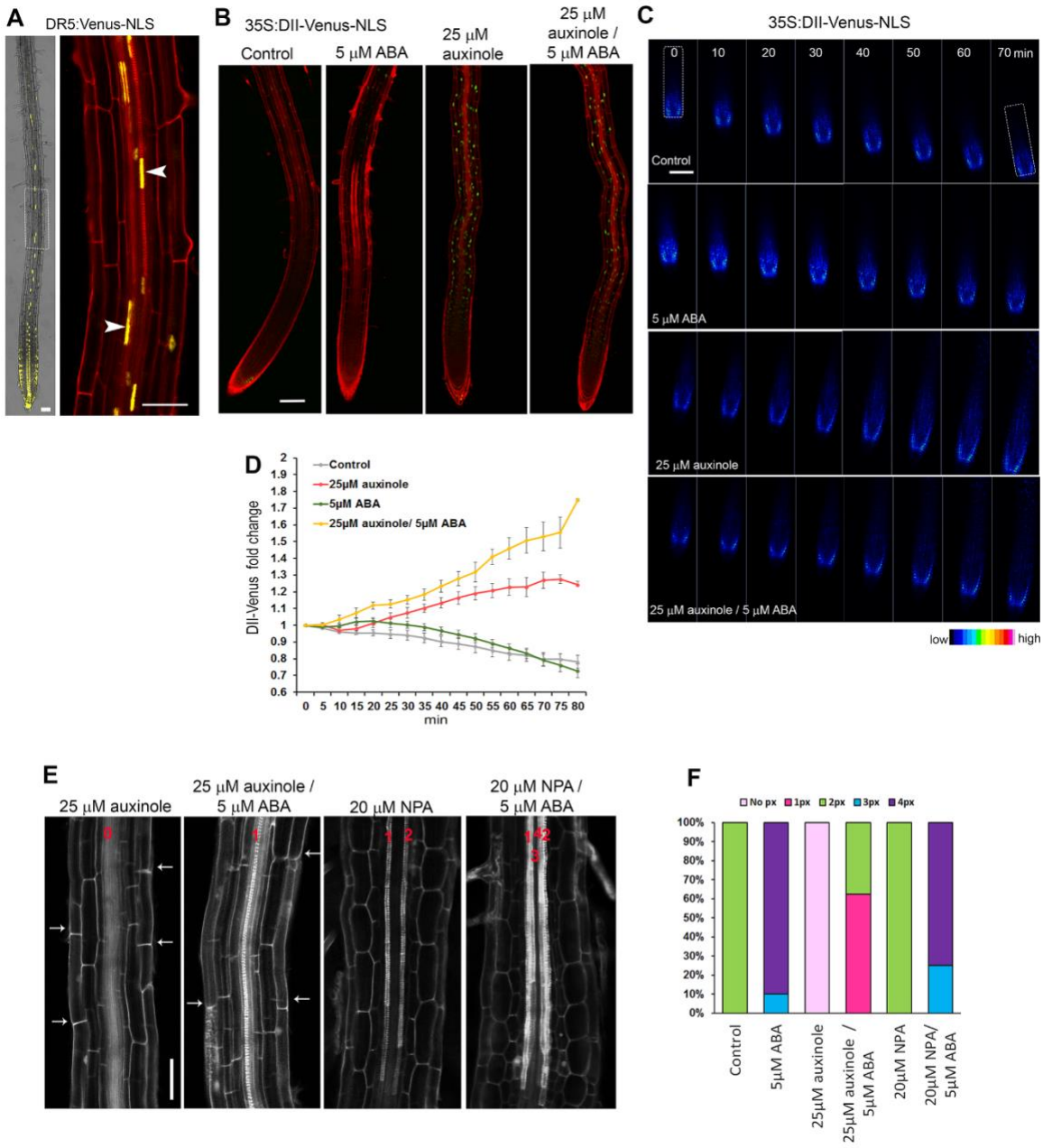

Fig. S11. **ABA induces differentiation of additional PX when auxin signaling or transport are repressed by drug treatments.** *(A)* Expression pattern of DR5::Venus-NLS (yellow). Cell walls were stained with PI (red). Left panel, DIC/fluorescence overlay. The dashed rectangle marks the enlarged region shown to the right. Arrowheads indicate elongated nuclei that are typical of differentiating PX cells. Note that in the maturation zone Venus-NLS expression is primarily detected in the PX. *(B)* The effect of 24-h treatment with indicated agent on the expression of 35S::DII-Venus (green). Cell walls were stained with PI (red). Auxinole treatment resulted in increased DII-Venus fluorescence. *(C)* Time series of representative *35S::DII-Venus* roots following application of ABA and auxinole. DII-Venus fluorescence is represented as a range of intensities.

White rectangles mark regions of root that were used for quantification in panel D. (*D*) Fold change (relative to time 0, which was taken as 1) in DII-Venus fluorescence intensity after application of ABA and auxinole at the indicated concentrations (n=5-6 roots /treatment). (*E*) Vascular tissue composition following 24 h treatments at the indicated concentrations of drugs and hormones. Note induction of PX differentiation by ABA in auxinole treated plants and inhibition of root hair emergence (arrows) with auxinole. (*F*) Frequency of PX formed following the drug and hormone treatments described in panel D (n=8-10/treatment). *S*cale bars in panels *A*, *B* and E, 50 μm and 100 μm in *C*.

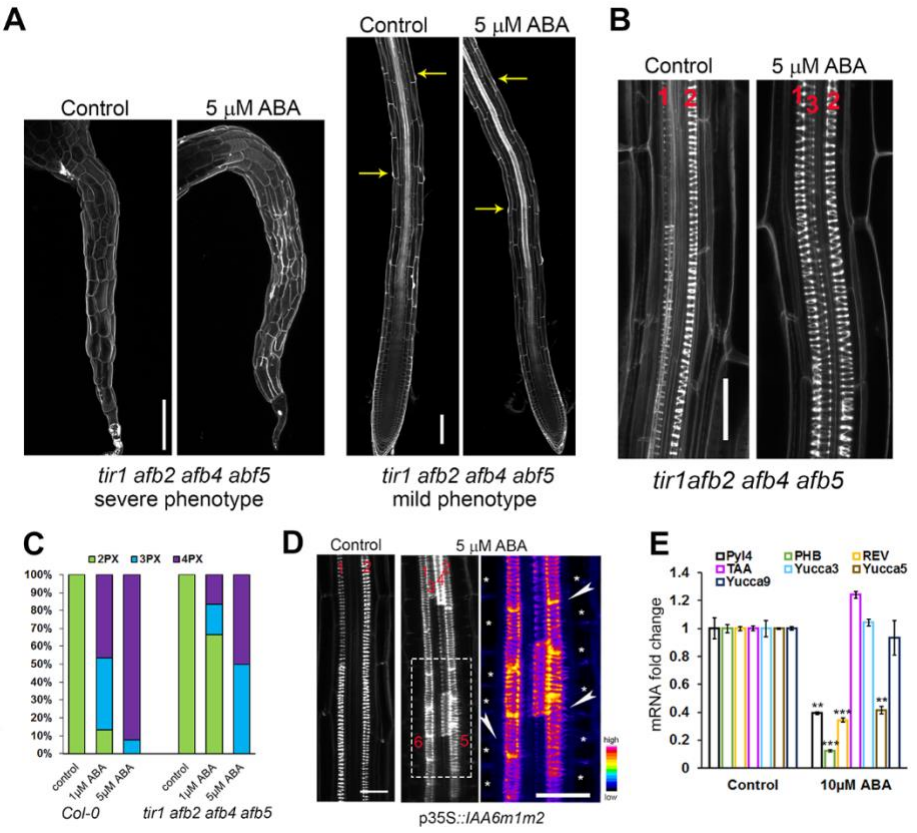

Fig. S12. **ABA response in auxin signaling mutants and effect on expression of auxin biosynthesis genes.** *(A)* Strong and mild phenotype of *tir1;afb2;afb4;afb5* mutant with and without ABA treatment. Note that in mutants with mild phenotype only emerging but not grown root hairs (yellow arrows) are detected, in agreement with compromised auxin signaling in this mutant. (*B*) PX differentiation in *tir1;afb2;afb4;afb5* mutant 24 h following incubation in control or 5 µM ABA media. (*C*) Frequencies of additional PX files formed in *tir1;afb2;afb4;afb5* compared to *Col-0* (*Col-0* n=8-10; *tir1;afb2afb4;afb5* n=9 per treatment). (*D*) PX differentiation in p*35S::IAA6m1m2* treated with 5 µM ABA. The far-right panel is an intensity range zoom of the region defined by the white dashed rectangle. Asterisks indicate endodermis, arrowheads indicate spiral SCW in the pericycle. (*E*) Q-PCR analysis of relative transcript levels in roots of auxin biosynthesis genes (TAA, YUCCA3, YUCCA5 and YUCCA9), *PHB*, *REV* and PYL4 after 3 h treatments with 10 µM ABA. ** p≤ 0.005; *** p ≤ 0.0005 Student's t-tests, two-tail distribution, unequal variance. Scale bars in panel *A*, 100 µm; in *B*, 20 µm; and *D* 50 µm.

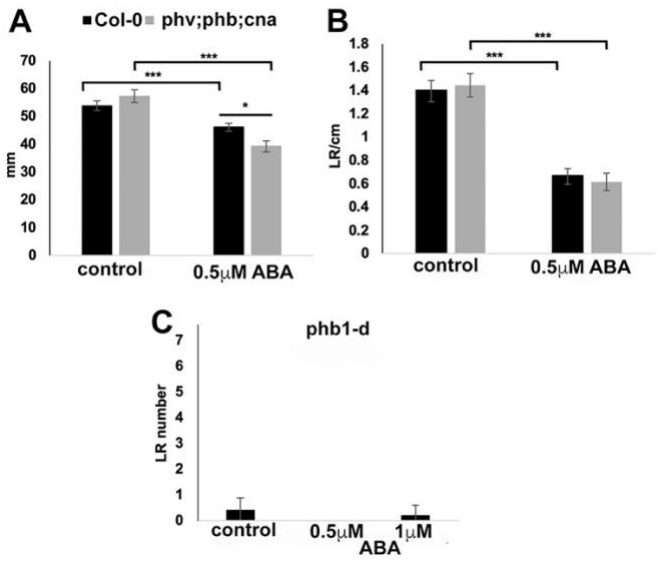

Fig. S13. **The effect of ABA on primary root length and lateral root density and number in triple HD-ZIPIII *phb phv cna* loss of function mutant and miR165/166 resistant *phb1-d* mutant.** A)primary root length of Col-0 and phb phv cna. B) Lateral root (LR) density of Col-0 and *phb phv cna*. C) Lateral root (LR) number in ph1-d. Control (ethanol). *p≤0.05, ***p≤0.0005 Student's t-test.

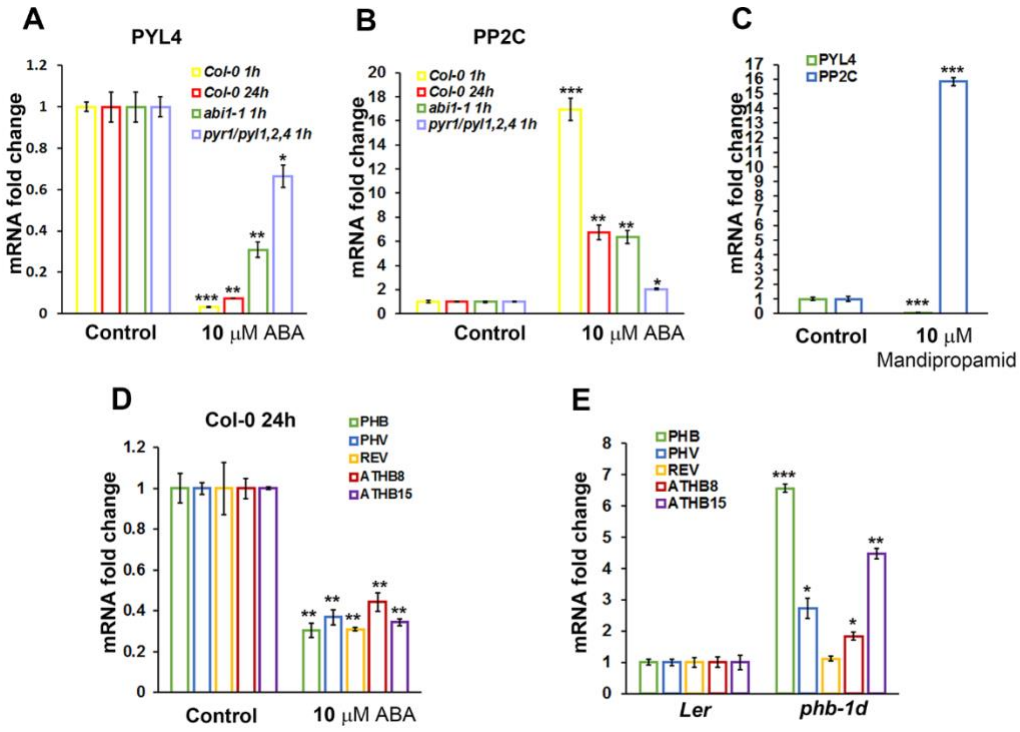

Fig. S14. **Q-PCR analysis of ABA responsive genes *PYL4* and *PP2C* and HD-ZIPIII mRNAs following treatments with ABA or mandipropamid.** (*A-B*) Relative transcript levels of *A*) *PYL4* and *B*) *PP2C* in *Col-0*, *abi1-1*, and *pyr1;pyl1;pyl2;pyl4* after 1 h and *Col-0* after 24-h treatments with 10 µM ABA. Note that after 24 h for *Col-0* or after 1 h for *abi1-1* and *pyr1;pyl1;pyl2;pyl4* the response to ABA of both *PYL4* and *PP2C* decreases compared to that of *Col-0* seedlings treated with ABA for 1 h. (*C*) Relative expression levels of *PYL4* and *PP2C* in *p35S:PYR1*^{MANDI} seedlings after 3 h treatment with 10 µM mandipropamid. (*D*) Relative transcript levels of HD-ZIPIII mRNAs following 24-h treatment with 10 µM ABA. (*E*) Expression of HD-ZIPIII mRNAs in *phb-1d* relative to *Ler* background. *p≤ 0.05; ** p≤ 0.005; *** p ≤ 0.0005. Student's t-tests, two-tail distribution, unequal variance. Error bars, SE.

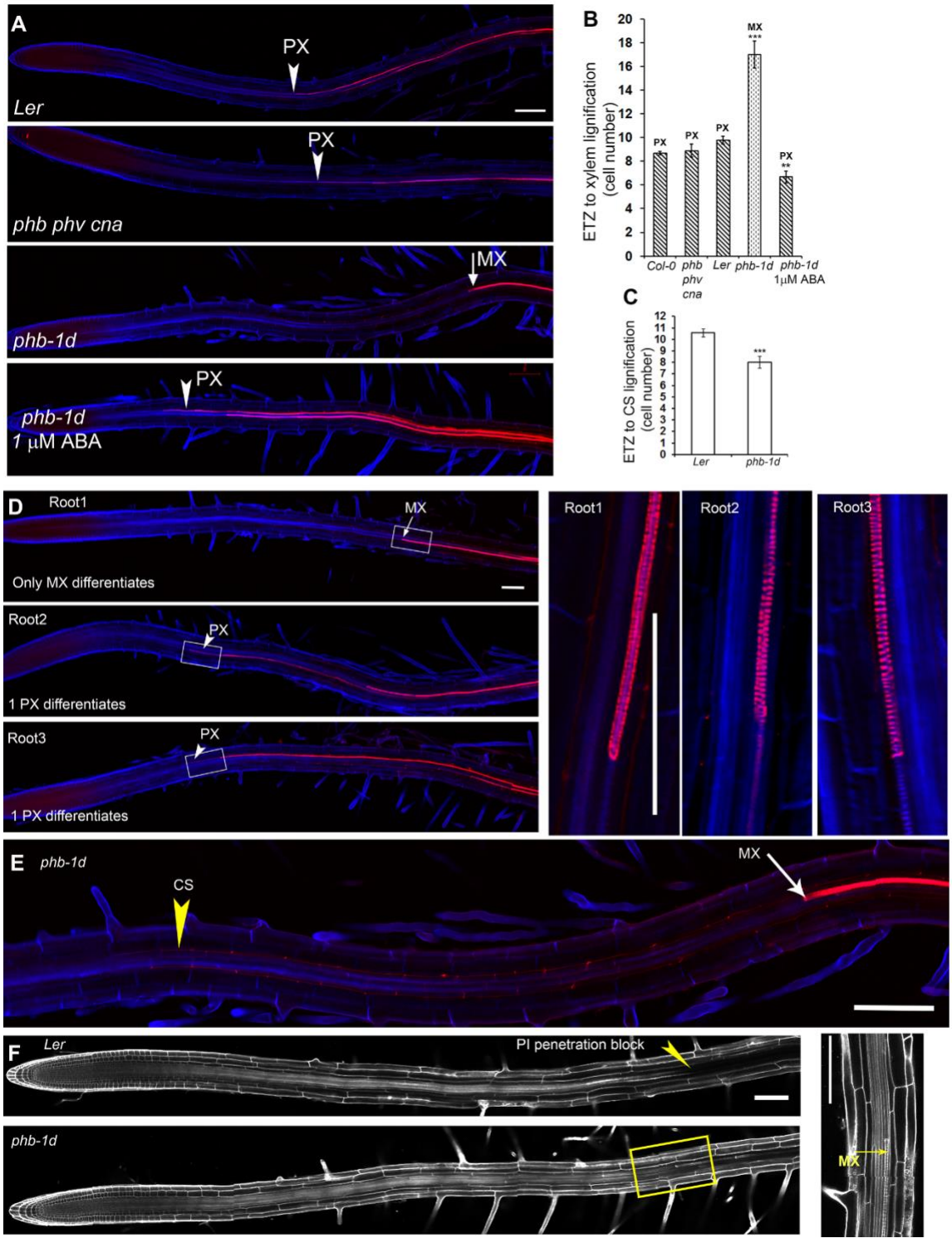

Fig. S15. **Phenotypes of *phb-1d* mutant.** (*A*) Cleared roots stained with calcofluor white (blue) for cellulosic cell wall and basic-fuchsin (red) for lignin. *Ler*, *phb;phv;can*, and *phb-1d* roots were imaged after growth in control conditions and *phb-1d* after 24-h treatment with 1 μM ABA. Positions of PX (arrowheads) and MX (arrow) lignification are indicated.

(*B*) Distance in cell number from ETZ to lignified SCW (PX or MX) (*Col-0* n=13*; phb;phv;cna* n=17; *Ler* n=16; *phb-1d* n=13; *phb-1d* treated with 1 µM ABA n=10). Statistical significance was calculated relative to *Ler*. (*C*) Distance in cell number from ETZ to Casparian strip lignification (*Ler* n=16; *phb-1d* n=13). (*D* and *E*) Cleared roots of *phb-1d* seedlings stained with calcofluor white (blue) and basic-fuchsin (red). (*D*) Root 1 is a representative image of xylem phenotype (13/15 roots) with no PX development and MX differentiation that starts in mature region of the root (17 cells from ETZ). Root 2 and Root 3 are representative of less frequent phenotypes (2/15) in which only one PX file develops and lignification starts 9 (Root 2) or 8 (Root 3) cells from the ETZ. Rectangles mark positions of enlarged areas shown at the right. (*E*) Frequent *phb-1d* phenotype depleted of PX differentiation but with normal differentiation of the Casparian strip (CS, yellow arrowhead). (*F*) *Ler* and *phb-1d* roots stained with PI (white). Yellow arrowhead indicates block of PI penetration into the stele due to penetration barrier formed by Casparian strip. Yellow rectangle in *phb-1d* marks region enlarged at the right where PI penetrates into the stele and stains MX (yellow arrow). Scale bars, 100 µm.

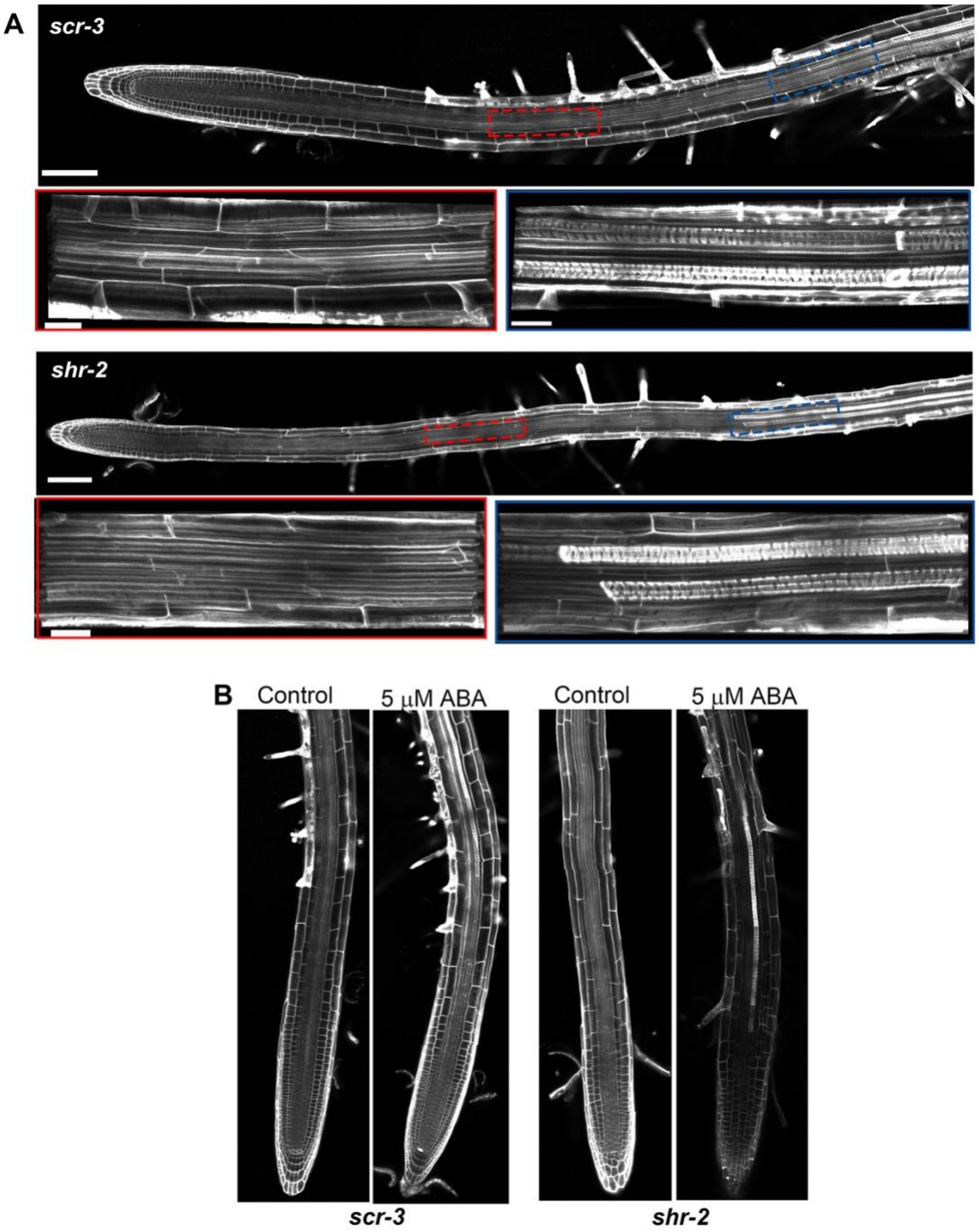

Fig. S16. **ABA treatments rescue PX specification in *shr2* and *scr3* mutants.** *(A) shr-2* and *scr-3* primary roots stained with PI (white). Red and blue dotted rectangles mark relevant enlarged regions. Note that in both mutants no PX differentiation was detected and MX differentiates later during development. *(B)* Effect of 24-h ABA treatments on PX differentiation. Note that ABA induced PX differentiation in both mutants. Scale bars in panels *A* 100 µm and 20 µm in enlarged regions, and in B 100 µm.

Table S1. Oligonucleotide primers used for quantitative RT-PCR (Q-PCR)

Gene accession	Primer name	Primer sequence 5`-3`
At3G11410	PP2C-For	TGGGATGGAGCTAGGGTTCT
	PP2C-Rev	CATACGGTTTCAAGTAATTATCACCA
At2G38310	PYL4-For	CGATCCGTAACGACCCTTC
	PYL4-Rev	CGACGTAAGACTCGACAACG
At2G34710	PHB-For	TTGGTTTCAGAACCGCAGA
	PHB-Rev	CTGTTTGAAGACGAGCAGCTT
At1G30490	PHV-For	TTGGTTCCAGAATCGCAGA
	PHV-Rev	CACTGTCTGAAGACGAGCTGA
At5g60690	REV-For	CGAGCTTGTTTATATGCAGACG
	REV-Rev	GCCAGATAGCGACCTCTCAC
At4G32880	ATHB8-For	CTCAAGAGATTTCACAACCTAACG
	ATHB8-Rev	TCACTGCTTCGTTGAATCCTT
At1G52150	ATHB15-For	CCGTCAACATACTCCAAATCC
	ATHB15-Rev	GTCACCACCGATTCACAGC
At1G70560	TAA1-For	GCCGCTCCTTTTTACTCCA
	TAA1-Rev	TGTACATACCCGACCGAACA
At1G04610	YUCCA3-For	ATCCGGTGGAAGGTACCAA
	YUCCA3-Rev	CCATACCGGAGTTTCCACAT
At5G43890	YUCCA5-For	AATCTCCATGATGTTGATGAAGTG
	YUCCA5-Rev	TCAGCCATGCAAGAATCAGT
At1G04180	YUCCA9-For	GGGCTATGGAGGGTTAGAACA
	YUCCA9-Rev	ACCAACCACCGGCAAATA
At1G13320	PP2A-For	TAACGTGGCCAAAATGATGC
	PP2A-Rev	GTTCTCCACAACCGCTTGGT

Table S2. Resources

Chemicals		
Murashige & Skoog (0.5X MS) salt mixture	Sigma-Aldrich	#M5519
+(-)cis, trans-abscisic acid (ABA)	Duchefa Biochemie	#A0941
α-naphthaleneacetic acid (NAA)	Sigma-Aldrich	#N-0640
auxinole	Ken-ichiro Hayashi, Okayama University of Science, Okayama, Japan	(Hayashi et al., 2008)
naphtylphtalamic acid (NPA)	Duchefa Biochemie	#132-66-1
poly(ethylene glycol, mol wt 8,000) PEG 8000	Sigma-Aldrich	#P5413
propidium iodide (PI)	Sigma-Aldrich	#P4864
Basic-Fuchsin	Fluka	#47860
calcofluor white	Sigma-Aldrich	#18909
Commercial Assays		
miRNeasy Micro Kit	Qiagen	217084
DNase	Qiagen	79254
High Capacity cDNA Reverse Transcription Kit	Applied Biosystems	4368814
Fast SYBR Green Master Mix	Applied Biosystems	4385612
***Arabidopsis* lines used in this study**		
Arabidopsis thaliana ecotype *Col-0*	ABRC	CS22625
Arabidopsis thaliana ecotype *Ler*	ABRC	
Arabidopsis thaliana ecotype *C24*	J. Dinneny	(26)
Col-0 35S::PYR1^{MANDI}	S. Cutler	(Park et al., 2015)
Col-0 abi1-1	ABRC	(Leung et al., 1994)
Col-0 pyr1;pyl1;pyl2;pyl4	S. Cutler	(Park et al., 2009)
Col-0 aba2-1	ABRC	(Gonzalez-Guzman et al., 2002)
Col-0 tir1-1;afb2-3;afb4-8;afb5-5	NASC	(Prigge et al., 2016)

Col-0 (er2) phb-13 phv-11 cna-2	ABRC	CS68977 (Prigge et al., 2005)
Col-0 scr-3	NASC	N3997 (Fukaki et al., 1998),
Col-0 shr-2	NASC	N2972 (Helariutta et al., 2000)
Ler phb-1d	J. Bowman	(McConnell et al., 2001)
Col-0 35S::Iaa6m1m2	E. Shani	(Li et al., 2011)
Col-0 pSCR::abi1-1	J. Dinneny	(26)
Col-0 pUAS::abi1-1	J. Dinneny	(26)
Col-0 pS18:ER-GFP	ABRC	(Lee et al., 2006)
Col-0 pVND7:GFP-NLS	T. Demura	(Kubo et al., 2005)
Col-0 pAHP6::GFP-ER	ABRC	(Bishopp et al., 2011)
Col-0 pMIR165a::GFP/pMIR166b::GFP	A. Carlsbecker	(Carlsbecker et al., 2010)
pPHB::GFP-ER	A. Carlsbecker	(Carlsbecker et al., 2010)
Col-0 pPHB:PHB-GFP	K. Nakajima	(Miyashima et al., 2011)
Col-0 DR5::Venus-NLS	M. Heisler	(Heisler et al., 2005)
Col-0 zll/pZLL::YFP:ZLL	T. Laux	(Tucker et al., 2008)
Col-0 DII-Venus	ABRC	(Brunoud et al., 2012)
C24 enhancer trap lines: J3411; J0951; J0571; Q2500; Q0990	J. Dinneny	(26)
Software		
Cell-O-Tape, CPIB macro-tool for Fiji (ImageJ)	(French et al., 2012)	
Fiji (Image J)		
Photoshop	Adobe	
ZEN	Zeiss	

References

Band, L. R., Wells, D. M., Larrieu, A., Sun, J., Middleton, A. M., French, A. P., Brunoud, G., Sato, E. M., Wilson, M. H., Peret, B., et al. (2012). Root gravitropism is regulated by a transient lateral auxin gradient controlled by a tipping-point mechanism. *Proc Natl Acad Sci U S A* **109**, 4668-4673.

Bishopp, A., Help, H., El-Showk, S., Weijers, D., Scheres, B., Friml, J., Benkova, E., Mahonen, A. P. and Helariutta, Y. (2011). A mutually inhibitory interaction between auxin and cytokinin specifies vascular pattern in roots. *Curr. Biol.* **21**, 917-926.

Brunoud, G., Wells, D. M., Oliva, M., Larrieu, A., Mirabet, V., Burrow, A. H., Beeckman, T., Kepinski, S., Traas, J., Bennett, M. J., et al. (2012). A novel sensor to map auxin response and distribution at high spatio-temporal resolution. *Nature* **482**, 103-106.

Carlsbecker, A., Lee, J. Y., Roberts, C. J., Dettmer, J., Lehesranta, S., Zhou, J., Lindgren, O., Moreno-Risueno, M. A., Vaten, A., Thitamadee, S., et al. (2010). Cell signalling by microRNA165/6 directs gene dose-dependent root cell fate. *Nature* **465**, 316-321.

Duan, L., Dietrich, D., Ng, C. H., Chan, P. M., Bhalerao, R., Bennett, M. J. and Dinneny, J. R. (2013). Endodermal ABA signaling promotes lateral root quiescence during salt stress in Arabidopsis seedlings. *Plant Cell* **25**, 324-341.

French, A. P., Wilson, M. H., Kenobi, K., Dietrich, D., Voss, U., Ubeda-Tomas, S., Pridmore, T. P. and Wells, D. M. (2012). Identifying biological landmarks using a novel cell measuring image analysis tool: Cell-o-Tape. *Plant Methods* **8**, 7.

Fukaki, H., Wysocka-Diller, J., Kato, T., Fujisawa, H., Benfey, P. N. and Tasaka, M. (1998). Genetic evidence that the endodermis is essential for shoot gravitropism in Arabidopsis thaliana. *Plant J* **14**, 425-430.

Gonzalez-Guzman, M., Apostolova, N., Belles, J. M., Barrero, J. M., Piqueras, P., Ponce, M. R., Micol, J. L., Serrano, R. and Rodriguez, P. L. (2002). The short-chain alcohol dehydrogenase ABA2 catalyzes the conversion of xanthoxin to abscisic aldehyde. *Plant Cell* **14**, 1833-1846.

Hayashi, K., Tan, X., Zheng, N., Hatate, T., Kimura, Y., Kepinski, S. and Nozaki, H. (2008). Small-molecule agonists and antagonists of F-box protein-substrate interactions in auxin perception and signaling. *Proc. Natl. Acad. Sci. USA* **105**, 5632-5637.

Heisler, M. G., Ohno, C., Das, P., Sieber, P., Reddy, G. V., Long, J. A. and Meyerowitz, E. M. (2005). Patterns of auxin transport and gene expression during primordium development revealed by live imaging of the Arabidopsis inflorescence meristem. *Curr Biol* **15**, 1899-1911.

Helariutta, Y., Fukaki, H., Wysocka-Diller, J., Nakajima, K., Jung, J., Sena, G., Hauser, M. T. and Benfey, P. N. (2000). The SHORT-ROOT gene controls radial patterning of the Arabidopsis root through radial signaling. *Cell* **101**, 555-567.

Kubo, M., Udagawa, M., Nishikubo, N., Horiguchi, G., Yamaguchi, M., Ito, J., Mimura, T., Fukuda, H. and Demura, T. (2005). Transcription switches for protoxylem and metaxylem vessel formation. *Genes Dev* **19**, 1855-1860.

Lee, J. Y., Colinas, J., Wang, J. Y., Mace, D., Ohler, U. and Benfey, P. N. (2006). Transcriptional and posttranscriptional regulation of transcription factor expression in Arabidopsis roots. *Proc Natl Acad Sci U S A* **103**, 6055-6060.

Leung, J., Bouvier-Durand, M., Morris, P. C., Guerrier, D., Chefdor, F. and Giraudat, J. (1994). Arabidopsis ABA response gene ABI1: features of a calcium-modulated protein phosphatase. *Science* **264**, 1448-1452.

Li, H., Tiwari, S. B., Hagen, G. and Guilfoyle, T. J. (2011). Identical amino acid substitutions in the repression domain of auxin/indole-3-acetic acid proteins have contrasting effects on auxin signaling. *Plant Physiol* **155**, 1252-1263.

McConnell, J. R., Emery, J., Eshed, Y., Bao, N., Bowman, J. and Barton, M. K. (2001). Role of PHABULOSA and PHAVOLUTA in determining radial patterning in shoots. *Nature* **411**, 709-713.

Miyashima, S., Koi, S., Hashimoto, T. and Nakajima, K. (2011). Non-cell-autonomous microRNA165 acts in a dose-dependent manner to regulate multiple differentiation status in the Arabidopsis root. *Development* **138**, 2303-2313.

Park, S. Y., Fung, P., Nishimura, N., Jensen, D. R., Fujii, H., Zhao, Y., Lumba, S., Santiago, J., Rodrigues, A., Chow, T. F., et al. (2009). Abscisic acid inhibits type 2C protein phosphatases via the PYR/PYL family of START proteins. *Science* **324**, 1068-1071.

Park, S. Y., Peterson, F. C., Mosquna, A., Yao, J., Volkman, B. F. and Cutler, S. R. (2015). Agrochemical control of plant water use using engineered abscisic acid receptors. *Nature* **520**, 545-548.

Prigge, M. J., Greenham, K., Zhang, Y., Santner, A., Castillejo, C., Mutka, A. M., O'Malley, R. C., Ecker, J. R., Kunkel, B. N. and Estelle, M. (2016). The Arabidopsis Auxin Receptor F-Box Proteins AFB4 and AFB5 Are Required for Response to the Synthetic Auxin Picloram. *G3 (Bethesda)* **6**, 1383-1390.

Prigge, M. J., Otsuga, D., Alonso, J. M., Ecker, J. R., Drews, G. N. and Clark, S. E. (2005). Class III homeodomain-leucine zipper gene family members have overlapping, antagonistic, and distinct roles in Arabidopsis development. *Plant Cell* **17**, 61-76.

Tucker, M. R., Hinze, A., Tucker, E. J., Takada, S., Jurgens, G. and Laux, T. (2008). Vascular signalling mediated by ZWILLE potentiates WUSCHEL function during shoot meristem stem cell development in the Arabidopsis embryo. *Development* **135**, 2839-2843.